Progress In Electromagnetics Research M, Vol. 97, 145–156, 2020

A Robust Approach for Three-Dimensional Real-Time Target Localization under Ambiguous Wall Parameters

Hua-Mei Zhang*, Sheng Zhou, Cheng Xu, and Jiao Jie Zhang

Abstract—To obtain three-dimensional (3-D) high-precision and real-time through-wall location under ambiguous wall parameters, an approach based on the extreme learning machine (ELM) which is a neural network is proposed. The wall's ambiguity and propagation effects are both included in the hidden layer feedforward network, and then the through-wall location problem is converted to a regression problem. The relationship between the scattered signals and the target properties are determined after the training process. Then the target properties are estimated using the ELM approach. Numerical results demonstrate good performance in terms of effectiveness, generalization, and robustness, especially for the kernel extreme learning machine (KELM) approach. Noiseless and noisy measurements are performed to further demonstrate that the approach can provide good performance in terms of stability and reliability. The location time, including the training time and test time, is also discussed, and the results show that the KELM approach is very suitable for real-time location problems. Compared to the machine learning approach, the KELM approach is better not only in the aspect of accuracy but also in location time.

1. INTRODUCTION

Detecting and localizing the hidden targets in enclosed structures are major challenges in a wide range of both civilian and military applications. The capability of electromagnetic (EM) waves to penetrate visually opaque obstacles provides an efficient means for sensing and seeing through obstacles. Through-wall radar imaging (TWRI) is such a non-destructive technique that has sparked growing interest.

During the past decades, several effective TWRI algorithms that consider the propagation phenomenology in layered media have been proposed, such as linear inverse scattering algorithms and the autofocusing approach based on the spectrum Green's function [1, 2]. A multi-algorithm fusion framework has also been presented to track human targets under the heterogeneity of walls and the scattering characteristics of human targets [3]. Another approach which decouples the through-wall localization problem into three separate components was proposed by Chen and Narayannan [4]. The approach improves the accuracy of target location estimation efficiently. Although successful imaging results and robust tracking performance can be obtained using these algorithms, they mainly deal with two-dimensional (2-D) scenarios that provide information on the range and azimuth profile. To obtain more valuable information about the target extent in length, width, and height, three-dimensional (3D) TWRI is proposed. Some researchers extend 2-D imaging to 3-D imaging. Ahmad et al. presented a delay-and-sum beamformer using line arrays for 2-D TWRI and a planar array for 3-D TWRI [5]. The height information was added to enhance target discrimination and identification abilities. To image targets behind multi-layered walls, Zhang et al. proposed full polarimetric beamforming algorithms based on the far field approximation of layered medium Green's function for 2-D and 3-D TWRI [6, 7]. To

Received 7 June 2020, Accepted 29 September 2020, Scheduled 16 October 2020
* Corresponding author: Hua-Mei Zhang (zhanghm@njupt.edu.cn).
The authors are with the College of Electronic Optical Engineering, Nanjing University of Posts and Telecommunications, Nanjing 210003, China.

obtain a 3-D image, Solimene et al. proposed a 2-D sliced approach that can be employed to obtain the 3-D scene by the superposition and interpolation of 2-D reconstructed images [8, 9]. Other researchers have provided successful 3-D imaging results directly. Using the time-domain approach, a comprehensive system-level simulation platform was proposed. Then, a backprojection microwave imaging algorithm was applied for 3-D focused images of radar targets [10].

Although the aforementioned algorithms are successful in obtaining satisfactory imaging, they are time-consuming in 3-D situations or large-scale scenarios. Due to the easy implementation of the algorithm with fast Fourier transform (FFT) and inverse FFT (IFFT), diffraction tomography (DT) has much higher computational efficiency [11]. Then, Zhang and Hoorfar proposed a 3-D DT algorithm based on the first-born approximation and the spectral expansion of the wall's dyadic Green's function for real-time through-the-wall radar imaging. The image is efficiently reconstructed and easily implied, which makes the diffraction tomographic TWRI algorithm suitable for on-site applications [12]. However, this real-time imaging approach requires a wall estimation procedure in advance. It does not work under unknown wall parameters.

Therefore, all of the above approaches for TWRI cannot simultaneously handle two key problems: unknown wall parameters and real-time imaging. Machine learning approaches, such as support vector machines (SVMs) and least-squares support vector machines (LS-SVMs), can locate targets under unknown wall parameters at a relatively fast speed [13]. The TWRI problem aims to find the target properties according to the received signals. The relationship between the target properties and received signals is nonlinear and ill-posed because of the presence of the wall. However, it can be easily obtained through the training process of the machine learning approach in [13]. However, in the training process, the learning speed is very slow, although the testing process is very fast. To improve the location speed, an alternative technique in the area of neural networks, extreme learning machines (ELMs), is proposed in this paper. Conventional neural networks, such as the back-propagation (BP) algorithm, are based on biological learning mechanisms. Their learning speed is very slow, and trivial human intervention is needed. These challenging issues are also faced by SVMs. ELMs can overcome these challenges. ELMs were proposed by Huang et al. in 2004 [14], and the work generalizes single-hidden layer feedforward neural networks (SLFNs), which randomly choose the input weights. Thus, the hidden layer of SLFNs needs not be tuned, and random computational nodes that may be independent of the training data can be applied. Then, the learning speed significantly improves. According to neural network theory, reaching a smaller training error, the smaller the norm of weights is, the better generalization performance the feedforward neural networks tend to have. Different from traditional learning algorithms for neural networks, the ELM tends to reach not only a smaller training error but also the smallest norm of output weights [15]. Thus, ELMs usually achieve similar or better generalization compared to other learning algorithms. In general, ELMs build some tangible links between machine learning techniques and biological learning mechanisms [16] and provide better generalization performance at a much faster learning speed with minimal human intervention [15]. ELMs are competitive techniques and have attracted increasing attention in both regression and classification applications.

In the standard ELM, the parameters of the hidden node remain fixed after being randomly generated. The only unknown parameters in SLFNs are the output weight vectors between the hidden layer and output layer, which can simply be resolved by ordinary least-square directly. Thus, training an SLFN is simply equivalent to finding a least-squares solution. It is a learning process based on the principle of empirical risk minimization, and overfitting cannot be avoided. The orthogonal projection method can be used to solve the above problems, and the solution is more stable and tends to have better generalization performance. However, learning efficiency is reduced according to optimizing the regularization parameters. If the hidden layer feature mapping is unknown to users, a kernel matrix for the ELM is introduced according to Mercer's conditions. Similar to SVMs, feature mapping need not be known, and instead, it uses its corresponding kernel function. Thus the computational complexity of the kernel ELM (KELM) is significantly reduced. Compared to the standard ELM, the KELM can effectively improve the generalization and stability by using kernel mapping instead of random mapping. Compared to the SVM, optimal solutions will tend to be easily achieved if the same kernels are used [16].

In TWRI, the relationship between the received signals and target properties can be determined by the training process of the ELM algorithm. Then, the target properties can be estimated through

the testing process. The total location time consists of the training time and testing time. Generally, the testing time is less than the training time. If the training time is short, the total time is not long. This advantage is beneficial for realizing real-time application in TWRI. Then, the ELM algorithm can simultaneously solve the two key problems with computational efficiency and reliability. To the best of our knowledge, the ELM for 3-D real-time automatic detection has not been addressed in prior works in the context of TWRI.

This paper proposes the ELM-based approach to perform the through-wall location problem. This paper is organized as follows. In Section 2, the 3-D imaging geometry of TWRI is presented. In Section 3, the theory of ELM is presented in detail. The fundamental theory of the proposed approaches is also presented. Section 4 provides some numerical examples, and the paper concludes in Section 5.

2. MATERIALS AND METHODS

Figure 1 shows a typical scenario for the 3-D through-wall location. The simulations are performed using the XFDTD software, in which the domain of the TWRI problem is discretized with finite-difference time-domain (FDTD) square cells of 1 cm length, and the time resolution is 16.68×10^{-12} s. The relative permittivity, thickness, and conductivity of a single layer wall are denoted as $\varepsilon_r = 3$, $d = 10$ cm, and $\sigma = 0.001$ S/m, respectively. The investigation domain is assumed to be a cuboid region behind the wall and is denoted as $D = [0, 2.0] \times [1.1, 2.0][0, 1.0]$ m^3. A spherical metallic target in the investigation domain is centred at (x_c, y_c, z_c) with a diameter of $\rho_c = 5$ cm. The receivers over a rectangular planar aperture are parallel to the wall and 0.5 m away from the front side of the wall. One transceiver located at (1.0, 0.5, 0.5) m transmits an ultrawide-band short pulse signal, which is a 1.2 ns Gaussian pulse modulated by a 1.5 GHz cosine wave. The signals are reflected by the wall and refract through the walls. The signals are also scattered by the target. Finally, the signals are received by receivers. The receivers are an 4×4 array. They are 0.5 m away from the wall and on the same side as the transceiver. The interval between the antennas is 0.2 m.

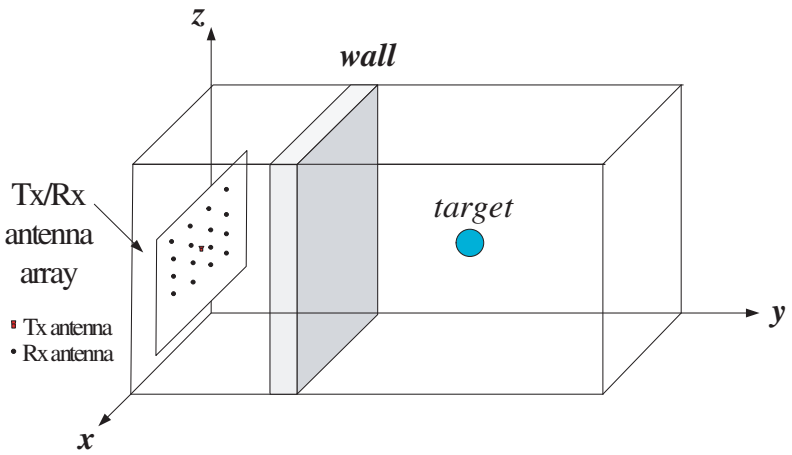

Figure 1. Schematic of through-wall geometry.

Then, the scattered signals introduced by the target are obtained by subtracting the electric field computed in the absence of the target from the total electric field computed in the presence of the target. The scattered signals of the target change with the location, shape, dielectric property, etc. In this paper, the location of the target is considered. Whether there is a target or not, one simulation requires approximately 5 minutes through XFDTD software. To obtain the scattered signals of the target, two simulations are needed. One simulation is in the scenes with the target and with the wall. Another simulation is in the scenes without the target but with the wall. The former simulation will repeat with the change of the location of the target, but the latter simulation only needs one time. If we want to obtain multiple (M samples) scattered signals of the target, all simulations need approximately

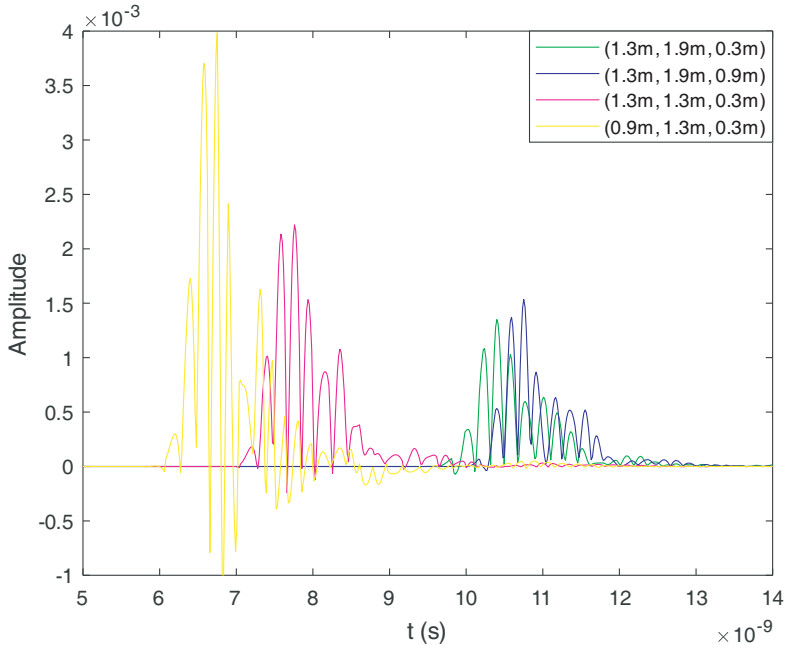

Figure 2. Amplitude of the received signal versus time for different locations.

$M \times 5 + 5$ minutes.

We assume that the scattered signals will merely change with the location of the target. Figure 2 shows the scattered signals versus the different centres of the target. From Figure 2, we know that the scattered signals will change in the x-direction, y-direction, and z-direction. Thus, there is some relationship between the scattered signals and target locations. However, the propagation phenomenology in layered media is more complex than that in free space, and the wall characteristics are also ambiguous. Thus, the relationship is nonlinear, uncertain, and inherently ill-posed. Then, the scattered signals can be considered as input, and the target locations can be considered as output. How to obtain the nonlinear relationship can be considered a regression problem. Once the relationship is confirmed, the location of the target can be obtained according to the scattered signals.

3. MATHEMATICAL MODE

Within the ELM framework, some arbitrarily distinct samples need to consist of the input array. In the TWRI problem, according to the analysis in Section 2, each centre location of the spherical target s represents a sample; that is, s represents x_c, y_c, or z_c. From Figure 2, we know that the maximum amplitude E and the corresponding time t are different when the target is in a different location. Then, they can be extracted as features of the target. For one sample, a one-dimensional vector $\mathbf{v} = (E_1, \ldots, E_n, t_1, \ldots, t_n)$ is obtained, where $n = 1, \ldots, N$ is the number of sampling points. Then the data $(\mathbf{v}, s)$ are obtained. When the target locations change, the data set in the form of $(\mathbf{v}_i,\ s_i)$ is generated, where i represents the ith sample. Then, in the ELM algorithm, a training set $\mathbf{W} = \{(\mathbf{v}_1, s_1), \ldots, (\mathbf{v}_l, s_l)\}$ is given, where $i = 1, \ldots, l$, l is the number of training samples; $\mathbf{v}_i = (E_{i1}, \ldots, E_{in}, t_{i1}, \ldots, t_{in}) \in \mathbf{R}^l$ is the input vector; and $s_i = [s_{i1}, s_{i2}, \ldots, s_{im}]^T \in \mathbf{R}^m$ is the output vector. The output function of the standard ELM is mathematically modelled as:

$$f(\mathbf{v}) = \sum_{i=1}^{L} \beta_i g_i(\mathbf{v_j}) \quad j = 1, \ldots, N \tag{1}$$

where $\beta = [\beta_1, \ldots, \beta_L]^T$ is the vector of the output weights between the hidden layer of L nodes and the output node, and g is the activation function. Because SLFNs can approximate these N samples

with zero error means, there exist $(\mathbf{a}_i, b_i)$ and β_i such that

$$f(\mathbf{v}) = \sum_{i=1}^{L} \beta_i G(\mathbf{a}_i, b_i, \mathbf{v_j}) = s_j, \quad j = 1, \ldots, N \tag{2}$$

where $G(\mathbf{a}_i, b_i, \mathbf{v_j})$ is a nonlinear piecewise continuous function. The above N equations can be written compactly as:

$$\mathbf{H}\beta = s \tag{3}$$

where

$$\mathbf{H} = \begin{bmatrix} \mathbf{h}(\mathbf{v_1}) \\ \vdots \\ \mathbf{h}(\mathbf{v_N}) \end{bmatrix} = \begin{bmatrix} G(\mathbf{a}_1, b_1, \mathbf{v}_1) \ldots G(\mathbf{a}_L, b_L, \mathbf{v}_1) \\ \vdots \ldots \vdots \\ G(\mathbf{a}_1, b_1, \mathbf{v}_N) \ldots G(\mathbf{a}_L, b_L, \mathbf{v}_N) \end{bmatrix} \tag{4}$$

$\mathbf{H}$ and $\mathbf{h}(\mathbf{v})$ are the hidden layer output matrix of the SLFN and the hidden layer feature mapping, respectively. In the standard ELM, from the interpolation capability point of view, the hidden layer parameters can be randomly generated if the activation function g is infinitely differentiable in any interval. Then Equation (3) is converted to solve the minimal norm least square:

$$\beta = \mathbf{H}^{\dagger} s \tag{5}$$

where $\mathbf{H}^{\dagger}$ is the Moore-Penrose generalized inverse of matrix $\mathbf{H}$.

In the orthogonal projection method, to improve the stability of the ELM, we have

$$\beta = \mathbf{H}^T \left(\frac{\mathbf{I}}{C} + \mathbf{H}\mathbf{H}^T \right)^{-\mathbf{1}} s \tag{6}$$

where C is a user-specified parameter. Then, the corresponding output function of ELM is

$$f(\mathbf{v}) = \mathbf{h}(\mathbf{v})\beta = \mathbf{h}(\mathbf{v})\mathbf{H}^T \left(\frac{\mathbf{I}}{C} + \mathbf{H}\mathbf{H}^T \right)^{-1} s \tag{7}$$

If the hidden layer feature mapping $\mathbf{h}(\mathbf{v})$ is unknown, we can define a kernel matrix for the ELM. Then, the hidden layer output matrix $\mathbf{H}$ is written as:

$$\mathbf{H} = \begin{bmatrix} \mathbf{h}(\mathbf{v}_1) \\ \vdots \\ \mathbf{h}(\mathbf{v}_N) \end{bmatrix} = \begin{bmatrix} h_1(\mathbf{v}_1) \ldots h_L(\mathbf{v}_1) \\ \vdots \ldots \vdots \\ h_1(\mathbf{v}_N) \ldots h_L(\mathbf{v}_N) \end{bmatrix}_{N \times L} \tag{8}$$

Thus, we can define a kernel matrix for ELM as follows:

$$\mathbf{\Omega_{ELM}} = \mathbf{H}\mathbf{H}^{\mathbf{T}} : \mathbf{\Omega_{ELMi,j}} = \mathbf{h}(\mathbf{v}_i) \cdot \mathbf{h}(\mathbf{v}_j) = K(\mathbf{v}_i, \mathbf{v}_j) \tag{9}$$

Similar to orthogonal projection to improve the stability of the ELM, we have β as Equation (6); then, the output function of the ELM can be written as:

$$y = \mathbf{h}(\mathbf{v})\mathbf{H}^T \left(\frac{\mathbf{I}}{C} + \mathbf{H}\mathbf{H}^T \right)^{-1} s = = \begin{bmatrix} K(\mathbf{v}, \mathbf{v}_1) \\ \vdots \\ K(\mathbf{v}, \mathbf{v}_N) \end{bmatrix}^{\mathbf{T}} \left(\frac{\mathbf{I}}{C} + \mathbf{\Omega_{ELM}} \right)^{-1} s \tag{10}$$

Through the kernel $K(\mathbf{v}_i, \mathbf{v}_j)$, the data $(\mathbf{v}_i, \mathbf{v}_j)$ in the lower-dimensional space can be converted to the inner product $\mathbf{h}(\mathbf{v}_i) \cdot \mathbf{h}(\mathbf{v}_j)$ in the higher dimensional space, and there is no relationship with the dimensionality of the hidden layer feature space. The number of hidden nodes L needs not be specified, and only $K(\mathbf{v}_i, \mathbf{v}_j)$ needs to be given to users. The radial basis function (RBF) $K(\mathbf{v}_i, \mathbf{v}_j) = exp\left(-\gamma \|\mathbf{v}_i - \mathbf{v}_j\|^2\right)$ is one of the kernel functions and is used in this paper. The kernel parameter γ is the variance in the kernel function, which is the only parameter that needs human intervention. Compared to the standard ELM, the KELM is more efficient and more stable.

According to the above discussion, if a new sample $\mathbf{v}$ is given, then the estimated value s is obtained. The core idea of the estimation algorithm based on KELM is revealed in Figure 3.

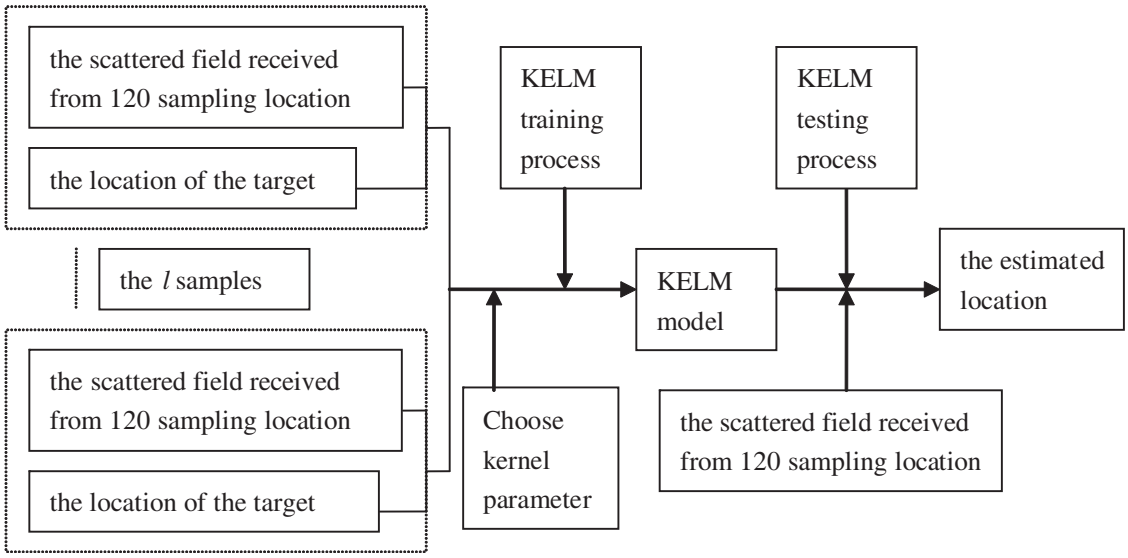

Figure 3. Flow chart of the estimation algorithm based on KELM.

4. RESULTS AND DISCUSSION

To show the efficiency and effectiveness of the proposed ELM algorithm for 3-D real-time through-wall location, some numerical simulations are presented in this section. In the simulation, the spherical target is assumed to be unchanged except for the change in the location, whose radius is 5 cm. Thus, the training data are achieved by repeated simulations with variation in the centre coordinates of the spherical target:

$$\begin{aligned} x_{train} &= 0.1 + n\Delta x, \quad n = 0, 1, \ldots, 9 \\ y_{train} &= 1.3 + m\Delta y, \quad m = 0, 1, \ldots, 3 \\ z_{train} &= 0.1 + k\Delta z, \quad k = 0, 1, \ldots, 4 \end{aligned} \tag{11}$$

where $\Delta x = \Delta y = \Delta z = 0.2$ m are sampling intervals which are same in this paper, but they can also be different. The sampling frequencies are 10, 4, and 5 respectively, and they are also independent. So there are 200 training samples.

In the same way, for testing samples, the centre coordinates of the spherical target vary as follows:

$$\begin{aligned} x_{test} &= 0.2 + n\Delta x', \quad n = 0, 1, \ldots, 8 \\ y_{test} &= 1.2 + m\Delta y', \quad m = 0, 1, \ldots, 3 \\ z_{test} &= 0.2 + k\Delta z', \quad k = 0, 1, \ldots, 3 \end{aligned} \tag{12}$$

where $\Delta x' = \Delta y' = \Delta z' = 0.2m$ are sampling intervals respectively. Similarly, they can be equal or unequal. There are 144 testing samples. The sampling frequencies are also independent. None of the test data are the same as the training data.

We first present a numerical example for the standard ELM with randomly generated hidden nodes and random neurons. In the training process of the standard ELM, the activation function and the number of random hidden neurons need to be known. Through simulations, we find that if the sigmoidal function is selected as the activation function, the best results will be obtained. Thus, the sigmoidal function is selected as the activation function in this paper. We also find that the larger the number of random hidden neurons is, the smaller the root mean squared error (RMSE) is. The RMSE is the mean value of the square root of error between the estimated value and true value. The smaller the RMSE is, the higher the estimated accuracy is. However, the calculation time will increase correspondingly. Thus, the number as large as possible under acceptable calculation time is chosen. Then, training model modelelm is obtained. According to modelelm, the testing data are used for

estimation, and the estimated results are shown in Table 1. From Table 1, we can see that the training time is approximately tens of seconds, the testing time is approximately a few seconds, and the RMSE is below 5 cm except in the width direction. Table 2 gives the estimated results of the KELM. In the KELM training process, the RBF is selected as the kernel function, and γ is the only parameter that needs to be tuned with the input data knowledge. In the simulation process, the optimal kernel parameter is selected when the RMSE is minimum. Then, the training data are trained by the KELM, and the model, which is called modelkelm, is obtained. From Table 2, both the training time and testing time are only a few milliseconds, and the RMSE is no more than 1.6 cm.

Table 1. Estimated results of standard ELM.

Location	Training time (s)	Testing time (s)	RMSE (cm)
length	50.453	3.703	4.054
width	45.781	3.609	14.889
height	19.094	1.438	2.872

Table 2. Estimated results of KELM.

Location	Training time (s)	Testing time (s)	RMSE (cm)
length	0.001	0.002	1.056
width	0.002	0.001	0.818
height	0.002	0.001	1.587

Table 3. Estimated results of SVM.

Location	Training time (s)	Testing time (s)	RMSE (cm)
length	26.018	0.886	3.217
width	87.712	0.809	14.362
height	86.252	0.799	2.971

To compare the ELM approach with the SVM approach, Table 3 gives the SVM results with the same simulation parameters. The RBF kernel function is used in the SVM. From Table 3, the training time is approximately tens of seconds; the testing time is no more than one second; and the RMSE is below 4 cm except for in the width direction.

In TWRI, the location time is a crucial problem. For this regression problem, the location time consists of the training time and testing time. In the training process, the standard ELM approach needs to search for the optimal number of hidden neurons, which is time consuming, while the KELM approach only needs to determine the appropriate kernel parameter. The SVM approach needs to optimize two parameters and requires more calculation time. Moreover, unlike machine learning approach, the training time of the ELM approach is not related to the number of training data, which is affected by the number of neural networks in the standard ELM and the kernel parameter in the KELM. Thus, if the number of samples is larger, the KELM approach can still train a model very fast. In general, the time on the order of seconds is sufficient. However, for the SVM approach, the training time significantly increases as the number of samples increases. For the standard ELM, the training time is longer than the time of the KELM approach but shorter than that of the SVM approach. The testing time will generally also be shorter than the training time. From Table 1 to Table 3, we can find that the training time of the KELM approach is four orders of magnitude shorter than that of the other two approaches, and the testing time is two orders of magnitude shorter than that of the SVM approach and three orders of magnitude shorter than that of the standard ELM approach. The KELM approach can obtain the most

accurate result with the fastest location speed. Thus even the 3-D schematic of through-wall geometry changes, on-site location is feasible because of the very short location time. Therefore, compared to the machine learning approach, the neural network approach is more suitable for real-time through-wall location.

To demonstrate the estimated results intuitively, Figure 4 gives the contrast between the estimated values and actual values. In Figure 4, the 45-deg diagonal line indicates that the estimated values are equal to the actual values. The round dots represent the estimated values of the standard ELM, and the stars represent the estimated values of the KELM. The closer the round dots or stars are to the diagonal line, the more precise the estimated values are. Figure 5 gives the error results between the actual values and estimated values quantitatively. In Figure 5, the estimated errors of length and width are under 2 cm, those of height under 3 cm for the KELM algorithm, and they are all under 6 cm for the standard ELM algorithm. From these statistical data, we know that all estimated accuracies of length, weight, and height are very high for the KELM algorithm. Moreover, regardless of the direction, the estimated results of the KELM algorithm are better than those of the standard ELM algorithm. The reason is that the KELM uses kernel mapping instead of random mapping which is used in the standard ELM, and the generalization and stability are effectively improved.

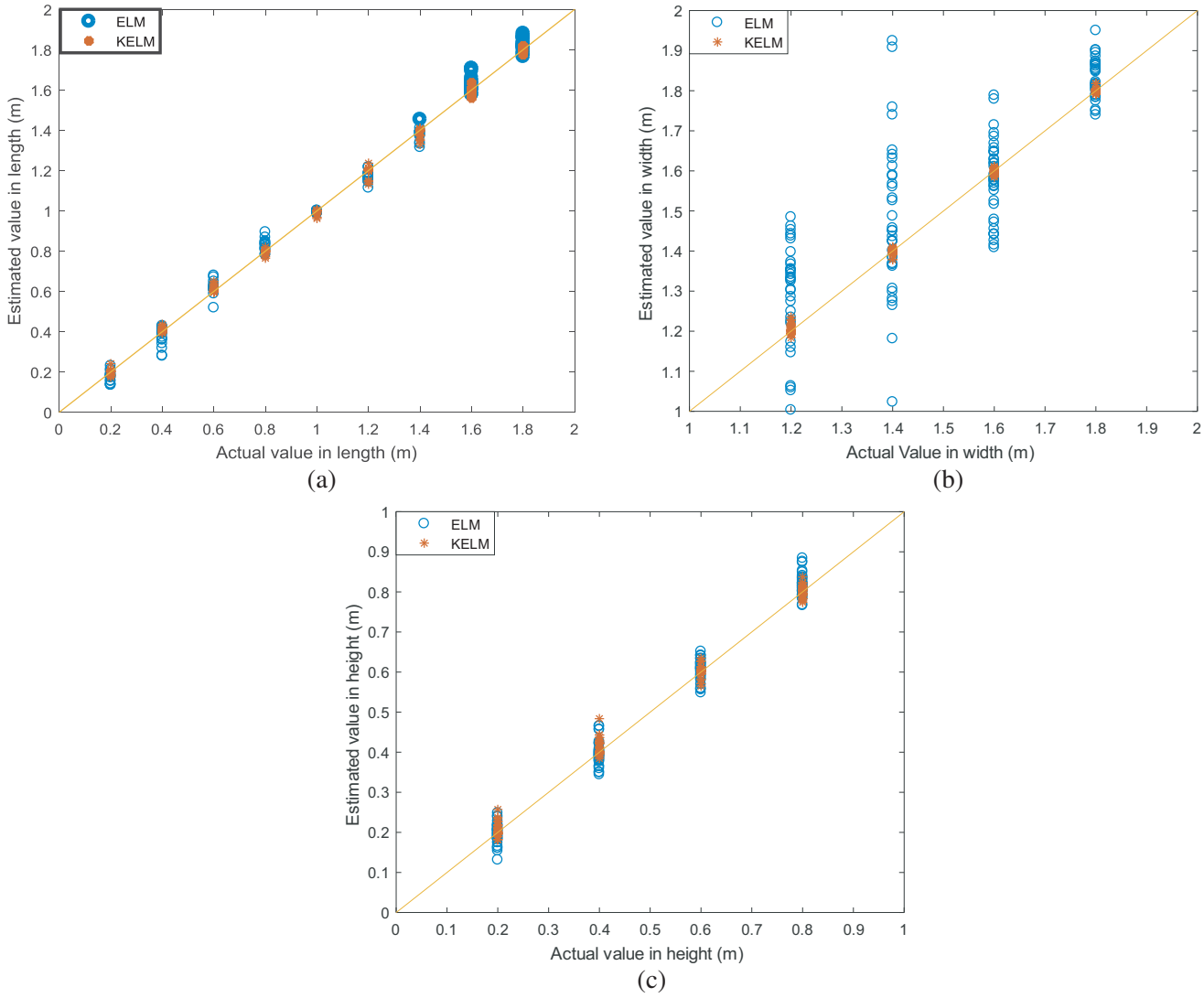

Figure 4. Estimated values of (a) length (b) width, and (c) height versus the actual values.

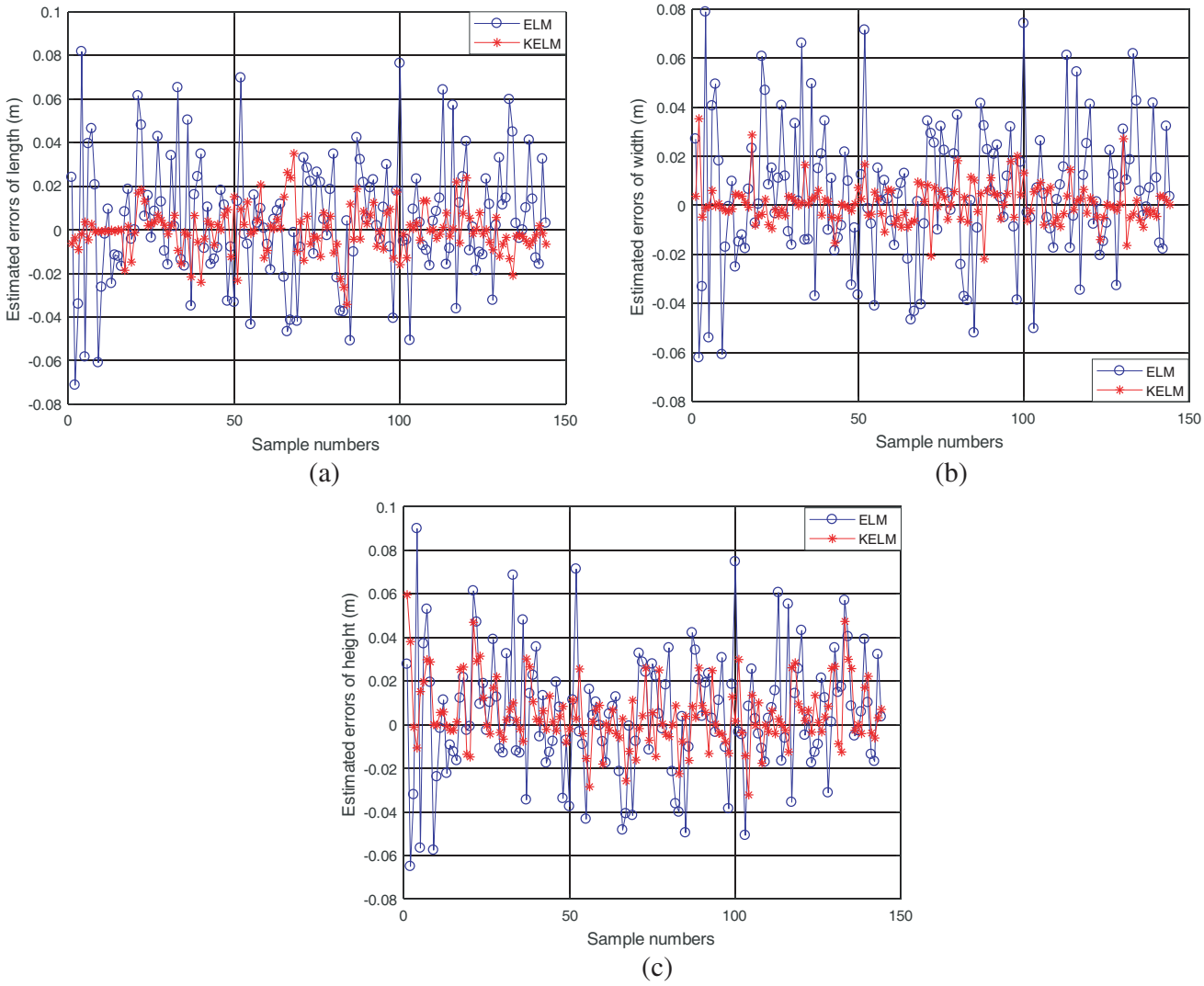

Figure 5. ELM algorithm versus KELM algorithm of (a) length (b) width, and (c) height.

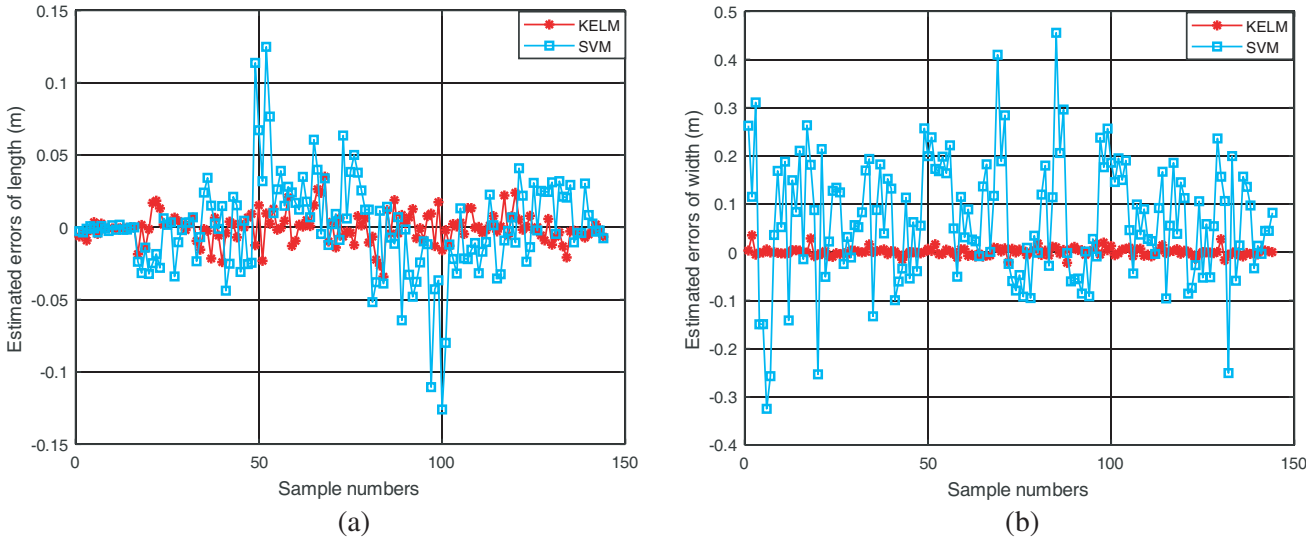

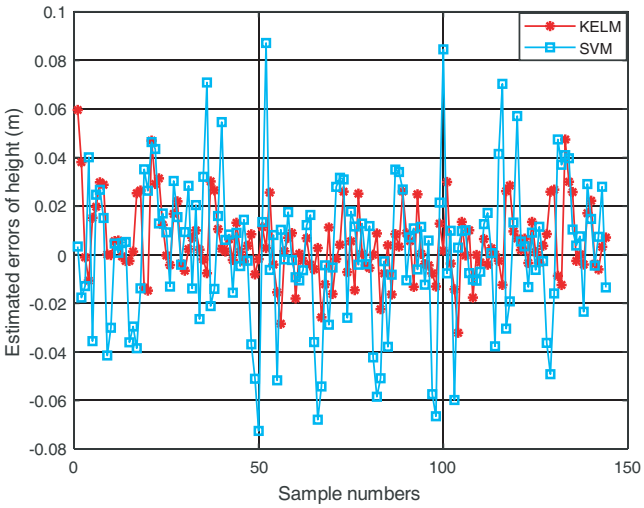

(c)

Figure 6. SVM algorithm versus KELM algorithm of (a) length (b) width, and (c) height.

To compare the accuracy of the ELM approach and SVM approach, Figure 6 gives the estimated errors of the KELM approach and SVM approach. In Figure 6, the estimated errors of length are under 5 cm, those of width under 30 m, and those of height are under 6 cm for the SVM approach. Thus in all directions, the results of the KELM are better than the results of the SVM approach, especially in the width direction. The KELM approach shows good performance in terms of accuracy and generalization.

To simulate more practical circumstances, Gaussian noise with a mean value of zero is added to the testing data, and all other parameters are the same as before. In this simulation, the signal-to-noise ratio (SNR) is set as 5, 10, 20, 30, 60, and 100 dB. The results of the mean error in the different directions are given in Figure 7.

Figure 7 shows that the ELM approach and SVM approach are almost unaffected by the added noise even through the SNR is very low, except in the width direction. However, the width direction is unaffected by the KELM approach. Under noisy circumstances, the mean error for the KELM algorithm is lower than that for the standard ELM algorithm and SVM algorithm in any direction. The KELM

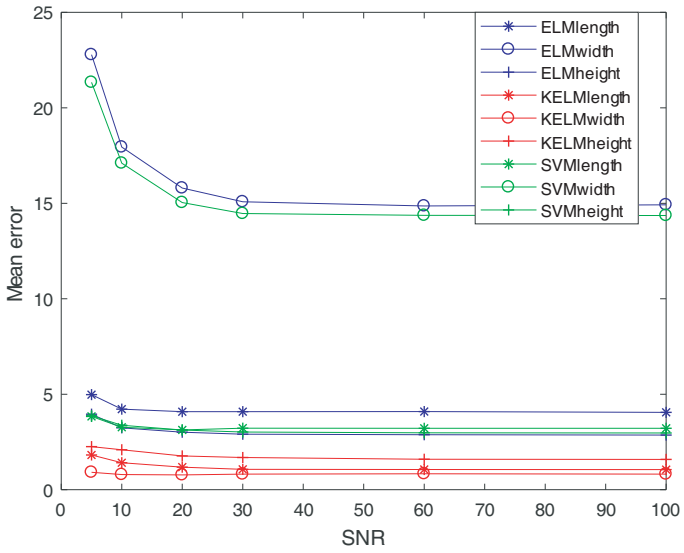

Figure 7. RMSE versus SNR.

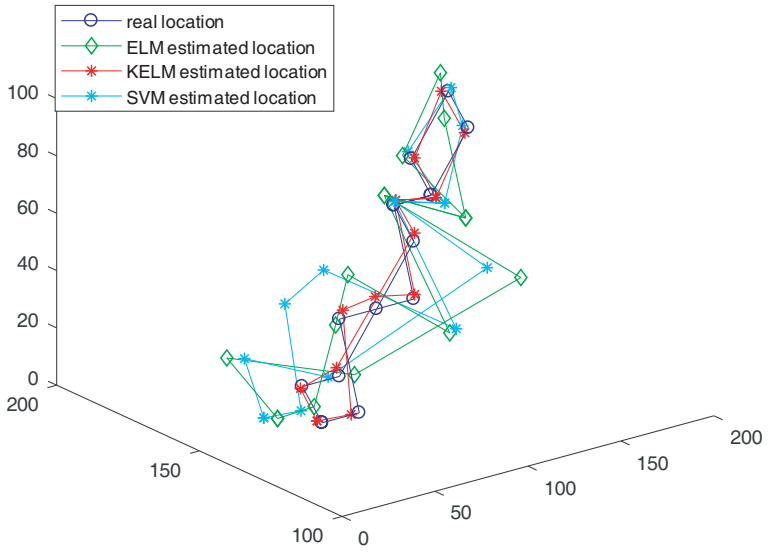

Figure 8. 3D target tracking.

approach is more robust than SVM approaches, such as supporting machine learning. Thus the KELM approaches present a competitive performance in through-wall location under noisy circumstances.

To verify the feasibility of the ELM approach, target tracking in a 3-D environment is simulated. The target moves along a random route. The tracking result is shown in Figure 8. From Figure 8, we know that the estimated route for the KELM approach almost coincides with the actual route, but those for the standard ELM approach and SVM approach deviate from the actual route. As a result, the KELM approach is competent in TWRI because of its high precision and real-time features.

5. CONCLUSIONS

The ELM approach for 3-D through-wall location under unknown wall parameters is proposed in this paper. The wall parameters' uncertainty and wall propagation effects are included in the hidden layer of the neural network. After the training process, the nonlinear relationship between the scattered signals that we can obtain directly and the target properties that we want to know are obtained. In this paper, the standard ELM approach and KELM approach are proposed, and their results are compared with those of the SVM approach. Because the kernel function in the KELM substitutes for the random neural number in the standard ELM, the accuracy of the KELM is higher, and the training time and testing time are shorter than that of the standard ELM, which are much shorter than that of the SVM approach. For the KELM approach, the estimated errors are under 0.02 m in length, width, and height, and both the training time and testing time are a few milliseconds. Thus the KELM approach demonstrates more speed and convenience in the training process and its good performance in terms of effectiveness and validity in automatic location. For both noiseless and noisy circumstances, the KELM approach provides stable results. In 3-D target tracking, the KELM approach can track the actual route reliably. Thus the KELM approach is very suitable for real-time location under unknown wall parameters.

However, the KELM approach is not suitable for the case of multiple targets. Future work will be aimed at locating multiple targets in a real-time process under unknown wall parameters.

6. FUNDING STATEMENT

This work is supported by the National Natural Science Foundation of China [Grant No. 61601242 61601245], Jiangsu Planned Projects for Postdoctoral Research funds [Grant No. 1601150C] and Jiangsu Government Scholarship for Overseas Studies [Grant No. JS-2017-026].

ACKNOWLEDGMENT

We want to thank the helpful comments and suggestions from the anonymous reviewers.

REFERENCES

1. Soldovieri, F. and R. Solimene, "Through-wall imaging via a linear inverse scattering algorithm," *IEEE Geoscience and Remote Sensing Letters*, Vol. 4, No. 4, 513–517, 2007.
2. Li, L. L., W. J. Zhang, and F. Li, "A novel autofocusing approach for real-time through-wall imaging under unknown wall characteristics," *IEEE Transactions on Geoscience and Remote Sensing*, Vol. 48, No. 1, 423–431, 2010.
3. Li, H. Q., G. L. Cui, L. J. Kong, et al., "Robust human targets tracking for MIMO through-wall radar via multi-algorithm fusion," *IEEE Journal of Selected Topics in Applied Earth Observations and Remote Sensing*, Vol. 12, No. 4, 1154–11648, 2019.
4. Chen, P. H. and R. M. Narayannan, "Shifted pixel method for through-wall radar imaging," *IEEE Transactions on Antennas and Propagation*, Vol. 60, No. 8, 3706–3716, 2012.
5. Ahmad, F., Y. M. Zhang, and M. G. Amin, "Three-dimensional wideband beamforming for imaging through a single wall," *IEEE Geoscience and Remote Sensing Letters*, Vol. 5, No. 2, 176–179, 2008.
6. Zhang, W. J., A. Hoorfar, C. Thajudeen, and F. Ahmad, "Full polarimetric beam-forming algorithm for through-the-wall radar imaging," *Radio Science*, Vol. 46, RS0E16-1-RS0E16-17, 2011.
7. Zhang, W. J., A. Hoorfar, and Q. H. Liu, "Three dimensional imaging of targets behind multi-layered walls," *IEEE International Symposium on Antennas and Propagation and USNC-URSI Radio Science Meeting (APSURSI)*, Chicago, 1–2, 2012.
8. Solimene, R., F. Soldovieri, G. Prisco, and R. Pierri, "Three-dimensional through-wall imaging under ambiguous wall parameters," *IEEE Transactions on Geoscience and Remote Sensing*, Vol. 47, No. 5, 1310–1317, 2009.
9. Solimene, R., F. Soldovieri, G. Prisco, and R. Pierri, "3D microwave tomography by a 2D slice based reconstruction algorithm," *IEEE Geoscience and Remote Sensing Letters*, Vol. 4, No. 4, 556–560, 2007.
10. Wang, Y. Z. and A. E. Fathy, "Advanced system level simulation platform for three-dimensional UWB through-wall imaging SAR using time-domain approach," *IEEE Transactions on Geoscience and Remote Sensing*, Vol. 50, No. 5, 1986–2000, 2012.
11. Wolf, E., "Three-dimensional structure determination of semi-transparent objects from holography data," *Optics Communications*, Vol. 1, No. 4, 153–156, 1969.
12. Zhang, W. J. and A. Hoorfar, "Three-dimensional real-time through-the-wall radar imaging with diffraction tomographic algorithm," *IEEE Transactions on Geoscience and Remote Sensing*, Vol. 51, No. 7, 4155–4163, 2013.
13. Zhang, H. M., Z. B. Wang, Z. H. Wu, F. F. Wang, and Y. R. Zhang, "Real-time through-the-wall radar imaging under unknown wall characteristics using the least-squares support vector machines based method," *Journal of Applied Remote Sensing*, Vol. 10, No. 2, 020501-1–020501-8, 2016.
14. Huang, G. B., Q. Y. Zhu, and C. K. Siew, "Extreme learning machine: a new learning scheme of feedforward neural networks," *IEEE International Joint Conference on Neural Networks*, 985–990, 2004.
15. Huang, G. B., Y. Lan, and D. H. Wang, "Extreme learning machines: a survey," *International Journal of Machine Learning and Cybernetics*, Vol. 2, No. 2, 107–122, 2011.
16. Huang, G. B., "An insight into extreme learning machines: random neurons, random features and kernels," *Cogn Comput*, Vol. 6, 376–390, 2014.